RSC Advances

PAPER

View Article Online
View Journal | View Issue

Cite this: *RSC Adv.*, 2025, **15**, 2988

A scalable and eco-friendly carbohydrate-based oleogelator for vitamin E controlled delivery†

Elizângela Hafemann Fragal,[ab] Lorenzo Metilli,[b] Frédéric Pignon [b] and Sami Halila *[a]

Received 14th November 2024
Accepted 23rd January 2025

DOI: 10.1039/d4ra08087d

rsc.li/rsc-advances

Supramolecular oleogels, in which low-molecular weight oleogelators self-assemble into various nanostructures through non-covalent interactions, have witnessed increasing research activity in various fields of science, including food, cosmetics or remediation of marine oil spills. Herein, we report a simple scalable and environmentally friendly carbohydrate-based oleogelator, namely, the sodium salt of *N*,*N*′-dimethyl β-*C* glucosyl barbiturate (**GlcBMe**) that self-assembles through sonication to induce the gelation of polar organic solvent and later of non-polar vegetable oils by cationic exchange with quaternary ammonium surfactants. Water-soluble **GlcBMe** was capable of forming self-assembled fibrillar network bridging insoluble particles in the oil by sonication in the presence of a small amount of water. The rheological properties are reinforced by *in situ* particle bridging with quaternary ammonium surfactants as evidenced by multi-scale structural analyses. IR analysis indicated that –OH (from carbohydrates) and –C=O (from barbituric ring) were involved in hydrogen bonding promoting the formation of a fibrous network. The oleogel presented a non-Newtonian system showing a shear-thinning behavior and thixotropic properties. Advantageously, these oleogels showed excellent control and slow release of the loaded-vitamin E in a pH-dependent manner.

Introduction

Oil-based gelling agents, so-called oleogelators or organogelators, are usually additives applied to thicken or solidify a lipophilic fluid to give a number of critical functions including shape, texture, stability, and sensorially for specific applications. They are widely used in many industries such as agrifood, cosmetics, and pharmaceuticals, but also in specialty industrial sectors such as lubricants, paints, greases, petrochemistry, *etc.*[1] Oleogelators, when dissolved or dispersed in a suitable oil, provide a continuous three-dimensional molecular network through various intermolecular non-covalent interactions to form a solid-like physical gel. These oleogelators can be split into two groups: low molecular weight oleogelators (LMOGs), which lead through self-assembly and entanglement of generated nanostructures to supramolecular oleogels,[2] and (bio) polymers-based oleogelators, that lead through entanglement of high molecular weight chains to macromolecular oleogels.[3] Biopolymers include polysaccharide derivatives (cellulose ethers, dextrin palmitate, or pullulan stearate) and proteins (egg albumin, soy or whey protein), while non-biodegradable polymer-based oleogelators are made, for instance, of poly(-ethylene) and its copolymers, poly(acrylic acid) copolymers or sodium allyl sulfonate copolymers. In spite of their wide utility, the main problems of using (bio)polymer-based oleogelators are, first, a 'clumping' effect during dissolution because of their high molecular weight that prevents good penetration of the oil and subsequently bad uniformity of the formulation, and second, the heating process during gelation that could be detrimental for some unsaturated oils that are sensitive to temperature, or impracticable with solvent of a low boiling point such as ethanol, ethyl acetate or others.

Therefore, reducing the molecular weight to obtain LMOGs that could jellify fatty phases in a cold process is of great interest. The range of structures known to be LMOGs is plentiful and multifarious – from *n*-alkanes, waxes, lecithin, 12-hydroxystearic acid to more complex synthetic ones (sorbitan stearate (Span® 60), 1,3 : 2,4-di-*O*-benzylidene-D-sorbitol (DBS), glyceryl fatty acid esters). They have already been useful for several industrial applications such as in food products to replace non-healthy trans/saturated fats, in cosmetics to prevent oil leakage or to stabilize emulsions, in dermo-pharmacy/cosmetic for enhanced transdermal penetration, and in plastic and paint industries as thickeners. However, most of these LMOGs need a heating–dissolution process for oleogelation. As previously mentioned, such a process is a disadvantage for many industrial applications. In addition, there is a general tendency to promote the replacement of petro-

[a]*Univ. Grenoble Alpes, CNRS, CERMAV, 38000 Grenoble, France. E-mail: sami.halila@cermav.cnrs.fr*

[b]*Univ. Grenoble Alpes, CNRS, Grenoble INP (Institute of Engineering Univ. Grenoble Alpes), LRP, 38000 Grenoble, France*

† Electronic supplementary information (ESI) available. See DOI: https://doi.org/10.1039/d4ra08087d

sourced materials by renewable resources in order to avoid or reduce the impact that process technologies and industrial products have on the environment.

As part of our program aimed at designing and synthesizing carbohydrate derivatives with controlled self-assembly abilities, we recently demonstrated that amphiphilic sodium salts of β-*C*-glycosyl barbiturates could induce supramolecular hydrogelation by screening the negative charge on the barbituric ring after a heating/cooling cycle.[4,5] Here, we report a simple, efficient, and an unprecedented one-step synthesis of an eco-friendly carbohydrate-based oleogelator, namely, *N*,*N*′-dimethyl β-*C*-glucosyl barbiturate (**GlcBMe**) that allows the formation of supramolecular oleogels induced by a short sonication time (cold process). Sodium salts of β-*C*-glycosyl barbiturates are easily accessible in water through a "green" Knoevenagel condensation between protecting-group-free carbohydrates and barbituric acid derivatives.[6,7] Structure–oleogelation property relationships were performed with a series of β-*C*-glycosyl barbiturate derivatives that highlighted the delicate balance between the nature of the *N*-substituents on the barbituric ring and the orientation of the hydroxyl groups on the carbohydrate. Finally, detailed mechanical properties and flow behavior were fully characterized to establish, in particular, the thixotropic nature of the oleogels. Moreover, vitamin E, as an antioxidant used for topical applications, was entrapped during the oleogelation and the differential *in vitro* release profile was performed.

Experimental methods

Materials

Fluorescein sodium salt, galactose, glucose, maltose, mannose, sodium bicarbonate ($NaHCO_3$), tetrabutylammonium bromide (TBAB), and 1,3-dimethylbarbituric acid and 1,3-dicyclohexylbarbituric were purchased from Sigma-Aldrich. Cetyltrimethyl ammonium bromide (CTAB) was purchased from Roth. Ethyl acetate was purchased from Biosolve. Ethanol and methanol were purchased from Carlos Erba. Almond oil was purchased from Ysiance, argan oil was purchased from Naturactive, and coconut and rosehip oil were purchased from Léa Nature (France). All chemicals were used as received without any further purification process.

General procedure for the synthesis of β-*C*-glycosyl barbiturate

The carbohydrate (1.1 M) and 1,3-dimethylbarbituric acid (1 equiv.) were dissolved in distilled water, followed by the addition of $NaHCO_3$ (1 equiv.) to reach a pH around 7, under magnetic stirring at 80 °C. The course of the reaction was monitored by thin layer chromatography (7 : 2 : 1 ethyl acetate/methanol/H_2O v/v/v). The reaction was stopped by cooling down the reaction at room temperature and precipitation by adding an ethanol/acetone (20/80 v/v) mixture. The resulting white solid was filtered out and washed two times with the same cosolvent mixture. Finally, the solid was dried under reduced pressure at 45 °C to afford a white powder (Fig. S1†). The yields for sodium salt of 5-(β-D-glycopyranosyl)-1,3-disubstituted barbiturate were in the range of 19% to 98%. The carbohydrate derivatives were fully characterized by ^{1}H NMR, and ESI-MS (see ESI†). ^{1}H NMR was recorded on a Bruker Advance DRX400 (400 MHz). Mass spectra (ESI-MS) were recorded using an Esquire 3000 spectrometer from Bruker.

Preparation of oleogels

Initially, for the formation of oleogels, oleogelators (2 wt%) were added to 0.5 mL of studied oil (argan, rosehip, almond, and coconut). After, the suspension was sonicated for 5 min to ensure adequate dispersion of the solid powders in the oil, and then 0.4 wt% of distilled water was added. The suspension was sonicated in an ultrasound bath (Elmasonic S 10H, Elma, Singen, Germany; 0.56 W cm^{-2}, 37 kHz) for 5 min and allowed to gelate as stated by inverting the vial. For the oleogels including surfactant particles cetyltrimethylammonium bromide (CTAB) or tetrabutylammonium bromide (TBAB) (1 molar equiv.), the same procedure was followed. The following abbreviations and compositions for the prepared oleogels are presented in the Table 1.

Infrared spectroscopy

IR spectra of the oleogelator and oleogels were analyzed using a PerkinElmer spectrometer. The oleogelator was analyzed in a powder state. Oil and oleogel samples were operated in attenuated total reflectance (ATR) mode. The samples were analyzed by transmission from 400 to 4000 cm^{-1}, resolution of 2 cm^{-1} with a total of 4 scans.

Differential scanning calorimetry measurements (DSC)

The thermal properties of oleogels were determined using a DSC (DSC Q200 TA instruments – New Castle, DE, USA). About 15–20 mg of oleogels was placed in a stainless-steel plate, and an empty plate was selected as a reference. The sample heating temperature was from 20 °C to 140 °C at a constant heating rate of 10 °C min^{-1} and then cooled from 140 °C to 20 °C at the same

Table 1 Abbreviation code related to the oleogel composition

Oleogel	Surfactant	Oil
[a]**GlcBMe** + Ar + H_2O–mix	—	Argan
GlcBMe–Ar	—	Argan
GlcBMe–C–Ar	CTAB	Argan
GlcBMe–C–Ro	CTAB	Rosehip
GlcBMe–C–Al	CTAB	Almond
GlcBMe–C–Co	CTAB	Coconut
GlcBMe–T–Ar	TBAB	Argan
GlcBMe–T–Ro	TBAB	Rosehip
GlcBMe–T–Al	TBAB	Almond
GlcBMe–T–Co	TBAB	Coconut

[a] **GlcBMe** – means oleogelator (sodium 5-(β-D-glucopyranosyl)-1,3-dimethylbarbiturate) and **GlcBMe** + Ar + H_2O–mix means mixture of **GlcBMe**, argan and H_2O without sonication; C = CTAB; T = TBAB, A = argan, Ro = rosehip, Al = almond and Co = coconut.

rate. Onset and peak temperatures were recorded. The melting parameters were obtained with TA Universal Analysis software.

In vitro release of vitamin E

Vitamin E-loaded oleogels were prepared by dispersing 2 wt% vitamin E into octyldodecanol oil (as a pure model oil-without vitamin E) under stirring until complete dissolution. Oleogelator (0.14 mmol) and 0.6 wt% of H_2O were added to the oil-vitamin. The mixture was sonicated for 5 min for oleogel formation. The *in vitro* diffusion rate of vitamin E was evaluated using the dialysis bag method. 0.5 mL of the oleogel was administrated through the syringe and then transferred into dialysis bags (10 kDa molecular weight cut-off). The dialysis bags were immersed in a beaker containing 30 mL of phosphate buffer (pH 7.4 and pH 5.5) containing 0.2 wt% Triton X-100 by continuous stirring at a speed of 200 rpm at 37 °C. At predetermined time intervals, 2 mL of releasing solution was removed for analysis and replaced by fresh PBS. The amount of vitamin E was analyzed by a UV-vis microplate TECAN spectrophotometer at a wavelength of 292 nm. These measurements were conducted in triplicate. Finally, vitamin E's content was calculated using the standard curve equation. The cumulative release percentage of the vitamin E was calculated as follows, eqn (1).

$$\text{cumulative release rate} = \frac{V_1 \times C_1 + V_2 \sum c_{i-1}}{m} \times 100\% \quad (1)$$

where V_1 is the total volume of the PBS (30 mL), C_1 is the concentration of the vitamin in the PBS solution ($\mu g\ mL^{-1}$), V_2 is the volume of the sample (2 mL), and m is the total quality of the composite oleogel. The amount of vitamin loading was 10 mg.

Statistical analysis

All values were reported as the mean ± error bars. Significant differences within the obtained data were determined using analysis of variance test (ANOVA) with a Tukey's *post-hoc* analysis at $p < 0.05$. All tests were performed using the origin software.

Results and discussion

As already discussed, in our continuous efforts to develop eco-friendly synthetic routes towards glycoconjugates and especially, glycoamphiphiles, we investigated the green Knoevenagel condensation of *N*,*N*′-substituted barbituric acid derivatives onto the reducing-end position of protecting-group-free carbohydrates. By this way, a series of amphiphilic β-*C*-glycosyl barbiturates have been found as efficient hydrogelators but never as LMOGs.[4] A serendipitous discovery was found with a simple and water-soluble sodium salt of *N*,*N*′-dimethyl β-*C*-glucosyl barbiturate (**GlcBMe**) that was first able to gelate, with a minimum gelation concentration (MGC) of 2 wt%, ethanol and secondly, other polar solvents were found such as glycerin, acetone, ethyl acetate, or butylene glycol. An inverted vial test, which is the usual indicative test of gelation, was used to assess the self-supporting gel formation (Fig. S31†). **GlcBMe** was easily synthesized by reacting commercially available glucose and *N*,*N*′-dimethyl barbituric acid in water at neutral pH for 4 h at 80 °C and purified by a simple precipitation in a remarkable quantitative yield. The synthesis was successfully upscaled up to 1 kg and the side products were only H_2O and CO_2, which met the criterion of green chemistry and of transposition to industrial scale. It is noteworthy that for gelation a small amount of water, around 0.4 wt%, was needed. This feature was already observed for some oleogelators such as lecithin where water was thought to induce a morphology transition from spherical to worm-like micelles and ultimately to a 3D network.[8–11] Since our **GlcBMe** organogelator is highly water-soluble, on the contrary of all others LMOGs, the role of water molecules should be likely to solubilize a part of **GlcBMe** required for effective self-assembled network formation. Originally, the gelation process includes traditionally a heating and cooling cycle. However, we found that our LMOG is able to gelate the above-mentioned solvents according to the traditional heating (90 °C)/cooling process but also in an energy-saving cold gelation process like sonication or just by mixing an aqueous high concentration of **GlcBMe** (14.7 M) injected in the organic solvent with a final 0.4 wt% of water. The common point of the three processes is the initial energy input (thermal, ultrasound or mechanical strength) allowing a disaggregation of the raw LMOG for a better solubility or dispersion in the organic solvent and for initiating an ordered arrangement through supramolecular interactions leading certainly to a mechanism of nucleation and growth of fibrils.

The discovery of our **GlcBMe** organogelator prompted us to investigate the structure/gelation property relationships by modifying selectively the nature of the carbohydrate or the *N*-substituent on the barbituric ring. The other potential LMOGs were synthesized in a similar manner by treatment of the corresponding carbohydrate (monosaccharide – glucose, mannose, galactose; disaccharide – cellobiose, maltose) with *N*,*N*′-disubstituted barbituric acid derivatives (*N*-methyl or *N*-cyclohexyl) in water at neutral pH and at 80 °C for 4 h (Scheme 1). The products were identified by 1D and 2D NMR, IR spectroscopy, and mass spectrometry (Fig. S2–S20†). The gelation tests showed no gelation properties for the series of synthesized β-*C*-glycosyl barbiturate derivatives and clearly evidenced the complexity of predicting LMOGs. Indeed, our results highlighted the fragile hydrophobic/hydrophilic balance needed to exhibit controlled aggregation without precipitation or complete solubility and the importance of the orientation of the carbohydrate hydroxyl groups for the non-covalent H-bond driving forces of gelation (Fig. S21†).

Gelation tests with less polar organic fluids such as edible oils were unsuccessful because of the high insolubility of our hydrophilic LMOG. Since our LMOG is a sodium salt of β-*C*-glucosyl barbiturate, we thought that by exchanging the sodium salt by an organic quaternary ammonium could compatibilized our LMOG to apolar solvents or oils. For such purpose, we used cetyltrimethylammonium bromide (CTAB) and tetrabutylammonium bromide (TBAB) which are also known as cationic surfactants. By this way, the gelation tests using sonication were successfully achieved with a wide range of vegetable oils such as

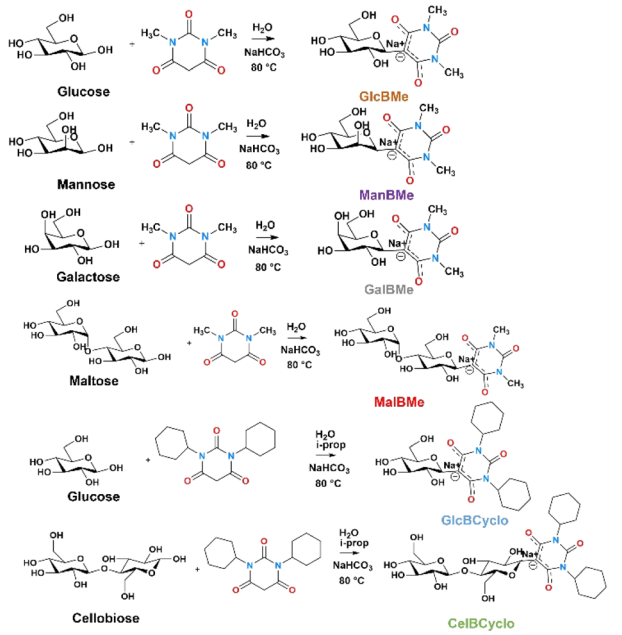

Scheme 1 Synthesis of sodium salt of *N,N′*-disubstituted β-*C*-glycosyl barbiturates.

argan, rosehip, almond, or coconut (Scheme 2). The MGC was still found to 2 wt% for all tested oils and the need of 0.4 wt% of water was still required. For the argan oil, the gelation occurred even without the need for organic quaternary ammonium (Scheme 2a), and no valuable explanations were found since the fatty acid composition of argan oil is roughly similar to those of almond oil.[12]

To deeper understand the role of each component before and after sonication, the microstructure of a mix of **GlcBMe**, water, and argan oil was visualized by confocal laser scanning (CLSM) and scanning electron microscopy (SEM). For improving the contrast between oil and water phases, a water-soluble fluorescein salt fluorophore was added. Before sonication, Fig. 1(a) (fluorescein stained) evidenced water droplets distributed non-homogeneously over the argan oily surface and SEM image revealed rod shape of as-prepared **GlcBMe** with

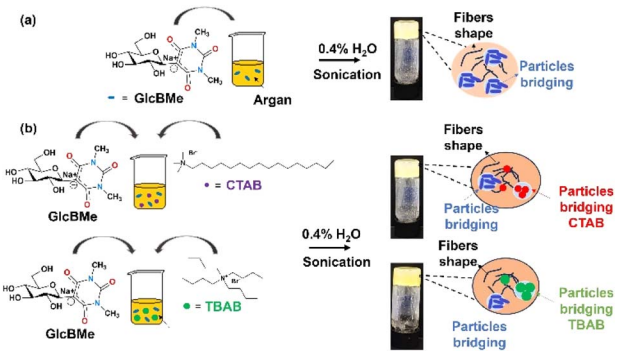

Scheme 2 Mechanism of formation of (a) **GlcBMe**-based oleogel in argan oil and (b) **GlcBMe**-based oleogels with cationic surfactants and different oils.

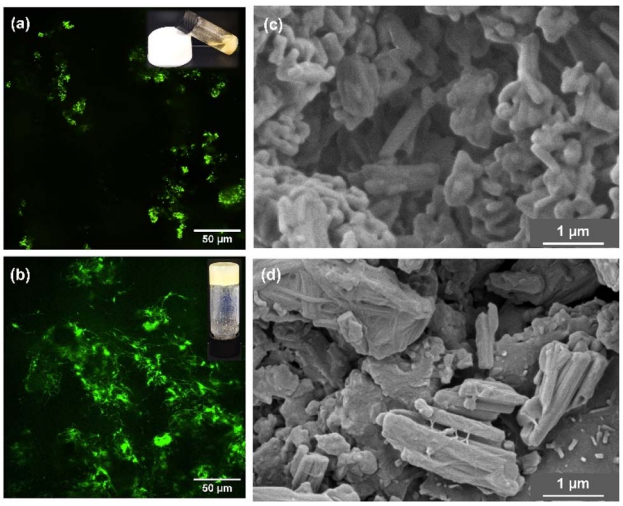

Fig. 1 CLSM microscopy images of (a) stained **GlcBMe** + Ar + H_2O–mix before sonication then (b) stained **GlcBMe**–Ar oleogel; and SEM images of (c) as-prepared **GlcBMe** then (d) **GlcBMe** oleogelator obtained from oleogel washed out with acetone.

a length of 0.55 ± 0.15 μm (Fig. 1(c)). While the sonication resulted in a more homogeneous dispersion of water and in mainly disaggregated **GlcBMe** areas (Fig. 1(b)). This suggests that sonication contributes to dissociate **GlcBMe** aggregates and to help in water penetration. This process allowed initiation of **GlcBMe** self-assembly towards a fibrillar network mixed with bridged **GlcBMe** microparticles as evidenced by SEM images (Fig. 1(d)) and as schematically illustrated in Scheme 2.

The same observations were pointed out for oleogels containing quaternary ammonium surfactants (CTAB or TBAB). Indeed, confocal images of a sonication-induced oleogel consisting in argan oil, CTAB, and **GlcBMe** oleogelator showed well-dispersed fibrillar structures encompassing granular CTAB crystals (Fig. S22†) and **GlcBMe** microparticles. The cationic surfactant particles in the "composite" or "hybrid" oleogel should act as additional physical cross-linking points in the network, presumably supported by ionic interactions between positively charged surfactants and the negatively charged surface of self-assembled **GlcBMe** fibers. This assumption was supported by the fact that non-ionic surfactants did not lead to oleogels.

XRD was used to evaluate the molecular assembly of **GlcBMe** and CTAB crystals in the **GlcBMe**–C–Ar oleogel, and the diffractograms are shown in Fig. S23.† The information about the order and the lateral packing of the molecular layers are provided by long spacing and short spacing peaks, respectively. Diffraction peaks in the XRD patterns of native **GlcBMe** and CTAB or the oleogel structured by **GlcBMe** and CTAB confirmed the presence of crystals, and their different spacing values indicated that the crystals had various structures, which were consistent with the results observed in SEM images. When oleogel is formed from the mixing of **GlcBMe** and CTAB in argan oil, we observed a broad diffraction signal around 20° 2θ, arising from the liquid crystal structuring of triacylglycerides of liquid argan (Ar) oil.[13] And the higher diffraction peak in the

long spacing region associated with the raw **GlcBMe** disappeared (48.5 Å), which indicated that a new self-assembly structure with fewer molecular layers was formed by **GlcBMe**. Noteworthy, several characteristic peaks for **GlcBMe** and CTAB were kept with slight shifts in *d*-spacing, suggesting that the subcell packing of **GlcBMe** and CTAB crystals were both modified in oleogel. It is reasonable to assume that in **GlcBMe**–C–Ar oleogel system, **GlcBMe** self-assembly and intimate mixture of crystal structures of **GlcBMe** and CTAB are the cause of oil gelation.

To further understand which molecular interaction occurred in the mixed crystals of **GlcBMe**, FTIR measurements were carried out. FTIR spectra of the oleogel samples (**GlcBMe**–Ar, **GlcBMe**–C–Ar, **GlcBMe**–T–Ar) as well as the raw materials (**GlcBMe** oleogelator, argan oil, CTAB, TBAB) and the mixture without sonication (**GlcBMe**–Ar–H_2O–mix) are shown in Fig. 2 for comparison. First observation, the oleogels did not reveal a new peak formation or peak disappearance revealing that simply physical interactions arose between the components. Next, the FTIR spectra of oleogels exhibited a shallow broad peak in the range of 3700–3100 cm^{-1} assigned to intermolecular H-bonding network of OH groups of glucose and amide bonds of barbituric ring that is not present for argan oil and surfactants (CTAB and TBAB). The oleogels, argan oil, CTAB and TBAB showed an absorption band around 2920 cm^{-1} and 2850 cm^{-1}, attributed to symmetrical and asymmetrical stretching of aliphatic C–H in CH_2 and CH_3 groups. The strong peak at 1750 cm^{-1} is characteristic of C=O stretching vibrations of the ester carbonyl functional group of the triglycerides of argan oil as usually observed with vegetable or edible oils.[14] Around 1680 cm^{-1} and 1580 cm^{-1}, it was possible to distinguish characteristic bands of C=O of amide constituting **GlcBMe**.[15] The argan oil-based oleogels shifted the position of the FTIR main peaks, with the most sensible ones about 1680 cm^{-1} and 1580 cm^{-1} (Fig. 2(b)), suggesting multiple molecular interactions between gelator–gelator, gelator–surfactants and gelator/surfactant–oil phase, including mainly intermolecular OH and C=O H-bondings and some van der Waals interactions.[16] Thus, a possible mechanism of intermolecular interaction pattern was proposed in Fig. 2(c). Since **GlcBMe** oleogelator is not soluble in fatty phases, self-assembled fibers and resulting gelation can be mainly attributed to hydrogen bonding, while with surfactants, van der Waals interactions and particle bridging play a contributive role, even though they are much weaker than hydrogen bonding.

Fig. 3 and S24,† along with Tables 2 and S1,† provide insights into the melting behavior of oleogels as characterized by DSC. Initially, **GlcBMe** and **GlcBMe**–Ar–H_2O–mix exhibited glass transition at approximately 76 °C and 63 °C, respectively, indicating changing from a hydrogen-bound system.[17] Notably, **GlcBMe** displayed a primary endothermic peak around 106.8 °C. Upon the addition of a small quantity of water without sonication (**GlcBMe**–Ar–H_2O–mix), the peak shifted slightly to 109.8 °C, suggesting a change in the melting process due to partial water-solubilization of **GlcBMe**, that disrupting the organization of **GlcBMe** crystals in the oil system. Following sonication and formation of **GlcBMe**–Ar oleogel, a single endothermic peak at 114.6 °C was observed, indicative of the formation of a more robust structure, likely associated to a self-assembly into a fibrillar network. The lower melting temperature (60–96 °C), observed after the addition of CTAB or TBAB particles to **GlcBMe**, may indicate the melting of intimate mixed crystals (**GlcBMe** and CTAB or TBAB), as shown in Fig. S24.† However, despite the expectation that the insertion of CTAB or TBAB particles would promote additional physical cross-liking points, valuable explanations for this behavior were not found, indicating that they had complex interaction mode. Additionally, the different studied oils led to a slight variation in endothermic peak position. This suggests that composition, polarity, and viscosity of the oil likely disturb the specific

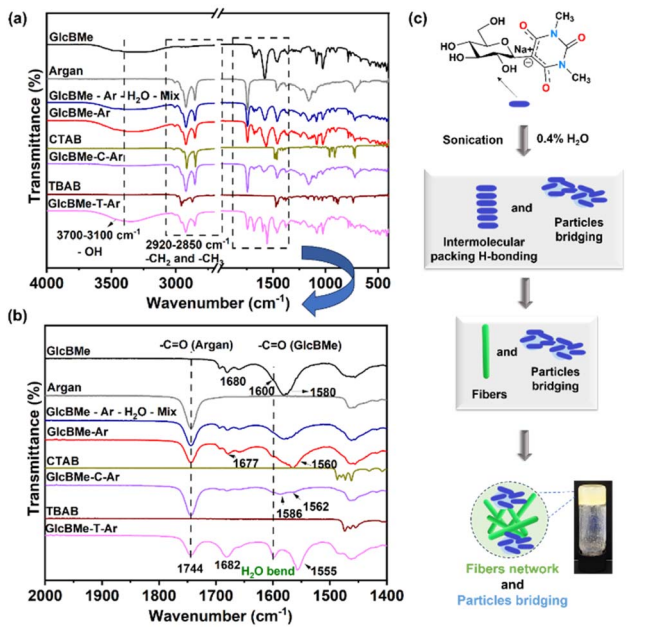

Fig. 2 (a) IR spectra (4000–450 cm^{-1}) and (b) (2000–1400 cm^{-1}) of **GlcBMe**, argan oil, **GlcBMe**–Ar–H_2O–mix, **GlcBMe**–Ar, CTAB, **GlcBMe**–C–Ar, TBAB and **GlcBMe**–T–Ar (c) illustration of self-assembly mechanism.

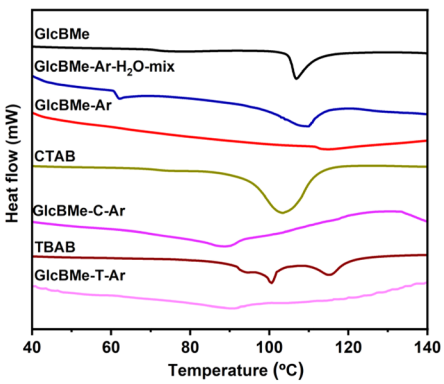

Fig. 3 DSC graph for **GlcBMe**, **GlcBMe**–Ar, **GlcBMe**–Ar + H_2O–mix, **GlcBMe**–Ar, CTAB, **GlcBMe**–C–Ar, TBAB, **GlcBMe**–T–Ar. *Analysis of **GlcBMe**, CTAB, and TBAB was made in oil.

Table 2 Melting temperature of samples

Samples[b]	T_{on}[a] (°C)	T_{peak}[b] (°C)
GlcBMe	104.8	106.8
GlcBMe–Ar–H_2O–mix	101.1	109.8
GlcBMe–Ar	111.8	114.6
CTAB	94.6	103.5
GlcBMe–C–Ar	72.6	88.6
TBAB	91.5/98.9/110.8	93.5/100.6/115.8
GlcBMe–T–Ar	66.6	89.6

[a] T_{on} – onset melting temperature. [b] T_{peak} – temperature of complete melting.

organization of mixed crystal and consequently influence the melting behavior.

Rheological studies were then carried out to have more information on the mechanical strength and the flow behavior of oleogels. Oleogels prepared by self-assembly and after addition or surfactant particles were examined in rheological studies at 25 °C. Fig. 4(a) shows the amplitude sweep for oleogel **GlcBMe**–Ar and with the addition of surfactant particles in argan oil, **GlcBMe**–C–Ar and **GlcBMe**–T–Ar, respectively. All samples showed the amplitude sweep which exhibited dominant solid behavior with $G' > G''$, with higher values for **GlcBMe**–C–Ar and **GlcBMe**–T–Ar samples. For **GlcBMe**–Ar the G' and G'' start to decrease until reaching a critical strain of 6.5% (where $G' = G''$). Above the critical strain, G' became smaller than G'', indicating the breaking of the structure and the initiation of the flow of the sample in accordance with the typical behavior of a yield stress jellified suspension. A frequency sweep was done to obtain more information, as shown in Fig. 4(b). The testing showed a predominance of elastic solid-like behavior ($G' > G''$), with an apparent elastic response across the full frequency range (detail data for other studied oils shown in Fig. S25a†).[18]

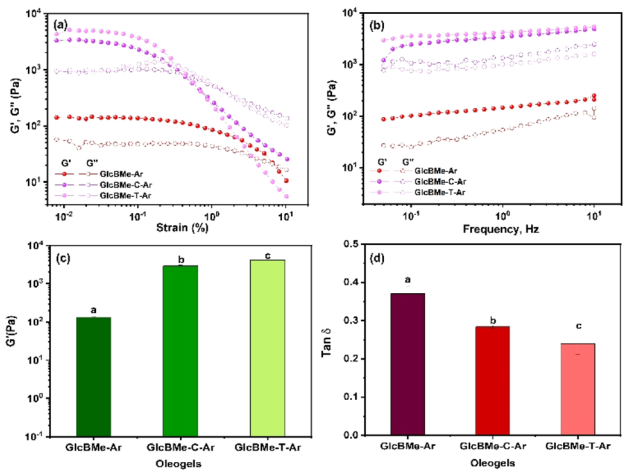

Fig. 4 Rheological behavior of oleogels (a) strain sweeps (b) frequency sweep (c) G' *vs.* oleogels (d) tan δ *vs.* oleogels for samples **GlcBMe**–Ar, **GlcBMe**–C–Ar, **GlcBMe**–T–Ar. Different letters assigned to each bar represent statistical differences between the values across all samples ($p < 0.05$).

The storage modulus (G') values corresponding to the plateau at low strain rate in the linear domain of Fig. 4(a) can effectively describe the mechanical strength of gels, and the corresponding values are reported in Fig. 4(c). Even **GlcBMe**–Ar exhibited higher G', the addition of surfactant particles, increasing the mechanical properties of oleogel with a significantly statistic difference ($P < 0.05$). The value with almost 1.0×10^{-5} Pa was rarely reported before with other LMWG (Table S2†),[19,20] resulting in higher overall resistance to deformation. The G' of the oleogels indicated their great potential to be used in applications requiring a semi-solid behavior. In Fig. S26a† we can note that the G' values of the oleogels were influenced by oil nature. In addition, the tan $\delta(G''/G')$ value was summarized in Fig. 4(d) and S26b.† It was found that the tan δ value of oleogel with surfactant particles was lower than **GlcBMe**–Ar, indicating the higher elasticity of oleogel after the insertion of surfactant particles. In terms of flow behavior, all samples displayed shear-thinning behavior since their viscosity declined gradually with the increasing shear rate (Fig. S27†). At the lowest shear rates, started the progressive disruption of the fiber network. With increasing shear rate, a complete breakdown of the fiber network displayed an orientation consistent with parallel flowing as evidenced by CLSM microscopy images in Fig. S28.†[21] This relatively higher viscosity at a low shear rate will bring better long-term stability of the oleogels during storage which is important for industrial applications.[22]

Further, the thixotropic nature was examined by step-strain measurement, to investigate to gain insights into the structural recovery. A two-step breakdown/buildup procedure was applied during the breakdown step and increase of strain from 0.03% to high magnitude strain (100%) was applied to destroy the oleogel, and then, in the buildup step a low magnitude strain (0.03%) was exerted to evaluate the rate and extent of recovery of bulk properties. To investigate the recovery of oleogel after breaking and reforming, the G' of recovering was shown in Fig. 5(a), (b) and S29–S30.† Interestingly, all oleogel reached 100% recovery, which is indicative of the impressive self-healing properties of the oleogel. Oleogel-based rosehip and surfactant particles was found to be able to rapidly recover the properties within 120 s, which demonstrated the reversible and robust nature of oleogel. More interestingly the recovery

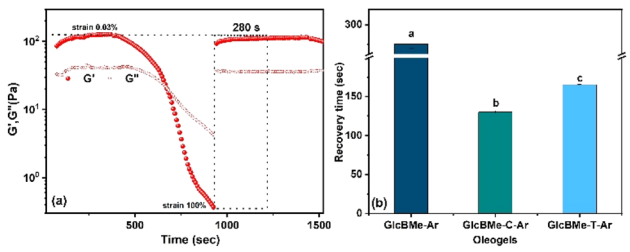

Fig. 5 (a) Thixotropic behavior for **GlcBMe**–Ar and (b) recovery time (s) in a two steps breakdown/buildup procedure for oleogel **GlcBMe**–Ar, **GlcBMe**–C–Ar, and **GlcBMe**–T–Ar *statistically differences between the values across all samples ($p < 0.05$). Different letters assigned to each bar represent statistical differences between the values across all samples ($p < 0.05$).

time seen in these oleogels is significantly influenced by the type of oil as well. The highest recovery G' was demonstrated by oleogels prepared with argan and coconut. The differences in recovery time in terms of different oils may be explained by changes in the polarity and level of unsaturation of the oil. The triacylglycerol (TAG) composition is an important factor. Argan oil for example, mainly presented unsaturated groups like oleo-dilinolein (OLL), dioleolinolein (OOL), palmito-oleio-linolein (POL), palmitodiolein (POO), and triolein (OOO), including oleic and linoleic,[23] suggesting that the unsaturated groups probably hinder the organization time of the fibers. It is clear that the oil type comprises diverse proportions of saturated and unsaturated fatty acids such as oleic acid (C18 : 1), linoleic acid (C18 : 2), palmitic acid (C16 : 0), and stearic acid (C18 : 0) (Table S3†). According to Kim *et al.*,[24] there is a correlation of the composition between the composition of oil in terms of the amount of C18 : 1 (oleic acid) and C18 : 2 (linoleic acid) fatty acids. Okuro *et al.*[25] highlighted the relationship between solvent polarity on mechanical strength, which is explained by the polar components of the oil phase's ability to interact with the oleogelator by creating hydrogen bonds.

Oil binding capacity (OBC) is an important property of oleogels, which is attributed to the amount of the oil that remains entrapped within the structure relying on the interactions between liquid oil and the gelator molecules. The oil binding capacity might be influenced by factors such as size, shape, and distribution of components in the network.[26,27] Oleogels-based different oils and surfactant particles were evaluated. Fig. 6(a) shows oleogels based on different oil and surfactant particles at a given oleogelator concentration. Oleogels-based rosehip showed a higher % OBC of around 60%. The higher percentage of OBC for oleogels-based rosehip showed a similarity to mechanical strength (G'). The percentage of OBC in oleogel samples on coconut was the lowest, around 20%. Considering different surfactant particles just for argan and almond oil showed some slight differences. However, the different type of oil seems to have more effect in % OBC, which probably in this system more branches and aggregates leading stronger 3D network which entraps liquid oil in the system.

The *in vitro* release behavior of the vitamin E (VE – a-tocopherol) model entrapped in the gel network was examined by the method of dialysis. VE is a natural antioxidant acting in cutaneous protective pathways against aging, atopic dermatitis, or melanoma, for instance.[28] It also widely used in food industry as a shelf-life enhancer of fatty products or to improve oxidative stability in heated oils. The release profile was carried out at two different physiological pH (7.4 and 5.5 (pH similar to the skin)) and similar behaviors were observed but with a higher release of VE at pH 7.4 (37% at 30 h) than at pH 5.5 (28% at 30 h) (Fig. 6(b)). A careful examination of the diffusion of VE through the lipid matrix of oleogels showed that during the first 2 h, a slight burst release of VE increased linearly for up to 15 h, after which the vitamin concentration remained constant. The higher release of VE at pH 7.4 compared to pH 5.5 is probably due to the higher solubility of VE at high pH, which increases the tendency of the drug molecule to leave toward the aqueous medium.

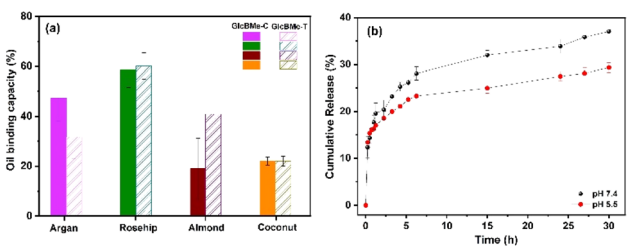

Fig. 6 (a) Oil binding capacity *vs.* different oil types at same gelator concentration (b) vitamin E release at pH 7.4 and 5.5 from oleogel GlcBMe–C.

Conclusions

In summary, a single-step and efficient green synthetic approach has been developed in order to design biosourced carbohydrate-based oleogelators. Indeed, Knoevenagel condensation in water of *N*,*N*′-disubstituted barbituric acids with unprotected carbohydrates led to a family of sodium salt of β-*C*-glycosyl barbiturates as potential organo-/oleo-gelators. Sodium salt of *N*,*N*′-dimethyl β-*C*-glucosyl barbiturate (**GlcBMe**) was discovered as a potent and unprecedented water-soluble organogelator, and oleogelator when cationic surfactants were added. Ultrasound-assisted gelation was successfully achieved with a wide range of organic solvents and oils owing to hierarchical self-assembly into entangled fibers and particles bridging. The investigation of the molecular structures–property of oleogelator suggested that hydrogen bonding is the key self-assembly driving force for the gelation even if the contribution of van der Waals interactions was established with cationic surfactants. Moreover, oleogels present outstanding mechanical strength, viscoelasticity, rapid recovery time after mechanical damage and oil binding capacity that are closely dependent to chemical composition of natural oils. Finally, our oleogels present great potential for active agent release for topical application. The eco-friendly and scalable preparation of the carbohydrate-based organogelator associated with robust and fast self-healable oleogel properties should provide an interest for an industrial transfer to many applications using fatty phases.

Data availability

The data supporting this article have been included as part of the ESI. See ESI for NMR spectra, microscopy images (optical microscopy, CLSM, TEM), DSC graphs and rheology data (Fig. S1–S31).†

Author contributions

Elizangela Hafemann Fragal: writing – original draft, conceptualization, methodology, investigation, formal analysis. Lorenzo Metilli: investigation, formal analysis. Frédéric Pignon: review, conceptualization, supervision, resources. Sami Halila:

writing – review & editing – conceptualization, supervision, resources.

Conflicts of interest

There are no conflicts to declare.

Acknowledgements

The authors acknowledge the financial support from the Institut Carnot PolyNat (ANR-21-CARN-0025-0). The author(s) acknowledge(s) the support of the French Agence Nationale de la Recherche (ANR), under grant ANR-21-CE07-0050 (SWEET-DISPLAY). We thank the CBH-EUR-GS (ANR-17-EURE-0003) and Glyco@Alps (ANR-15-IDEX-02) for additional supports. We acknowledge the NanoBio ICMG (UAR 2607) for providing facilities for mass spectrometry, NMR analyses and electronic microscopy.

References

1 H.-S. Hwang, *Biocatal. Agric. Biotechnol.*, 2020, **26**, 101657.
2 Z. Wang, J. Chandrapala, T. Truong and A. Farahnaky, *Crit. Rev. Food Sci. Nutr.*, 2022, **23**, 6069–6113.
3 Y. Li, Y. Zou, F. Que and H. Zhang, *Curr. Opin. Food Sci.*, 2022, **43**, 114–119.
4 S. Yao, R. Brahmi, F. Portier, J.-L. Putaux, J. Chen and S. Halila, *Chem.–Eur. J.*, 2021, **27**, 16716–16721.
5 S. Yao, R. Brahmi, A. Bouschon, J. Chen and S. Halila, *Green Chem.*, 2023, **25**, 330–335.
6 J. A. G. Perez, M. A. Gonzalez, J. L. J. Requejo and J. C. P. Albarran, *Carbohydr. Res.*, 1983, **124**, C15–C17.
7 F. Portier, J. Solier and S. Halila, *Eur. J. Org Chem.*, 2019, **36**, 6158–6162.
8 L. Wang, Y. Wen, C. Su, Y. Gao, Q. Li, S. Du and X. Yu, *RSC Adv.*, 2022, **12**, 8987–8995.
9 H. Xi and H. Zhao, *J. Mater. Sci.*, 2019, **54**, 4246–4258.
10 R. Scartazzini and P. L. Luisi, *J. Phys. Chem.*, 1988, **92**, 829–833.
11 Y. A. Shchipunov, *Colloids Surf., A*, 2001, **183–185**, 541–554.
12 P. K. Ojha, D. K. Poudel, A. Rokaya, S. Maharjan, S. Timsina, A. Poudel, R. Satyal, P. Satyal and W. N. Setzer, *Compounds*, 2024, **4**, 37–70.
13 A. Sadeghpour, M. L. Parada, J. Vieira, M. Povey and M. Rappolt, *J. Phys. Chem. B*, 2018, **122**, 10320–10329.
14 M. T. H. Swe and P. Asavapichayont, *Asian J. Pharm. Sci.*, 2018, **13**, 485–497.
15 M. A. Gonzalez, J. L. J. Requejo, J. C. P. Albarran and J. A. G. Perez, *Carbohydr. Res.*, 1986, **158**, 53–66.
16 M. Öğütcü, N. Arifoğlu and E. Yilmaz, *J. Am. Oil Chem. Soc.*, 2015, **92**, 459–471.
17 B. C. Baker, A. D. O'Donnell, Priya, M. Hyder, I. M. German and W. A. Hayes, *Eur. Polym. J.*, 2022, **162**, 110889.
18 V. Trappe and D. A. Weitz, *Phys. Rev. Lett.*, 2000, **85**, 449–452.
19 C. L. Esposito, V. Tardif, M. Sarrazin, P. Kirilov and V. G. Roullin, *Mater. Sci. Eng., C*, 2020, **114**, 110999.
20 M. Samateh, S. S. Sagiri, R. Sanni, C. A. Chee, S. Satapathy and G. John, *J. Agric. Food Chem.*, 2020, **68**, 13282–13290.
21 F. Pignon, M. Challamel, A. De Geyer, M. Elchamaa, E. F. Semeraro, N. Hengl, B. Jean, J. -L Putaux, E. Gicquel, J. Bras, S. Prevost, M. Sztucki, T. Narayanan and H. Djeridi, *Carbohydr. Polym.*, 2021, **260**, 117751.
22 D. Satapathy, D. Biswas, B. Behera, S. S. Sagiri, K. Pal and K. Pramanik, *J. Appl. Polym. Sci.*, 2013, **129**, 585–594.
23 S. Gharby and Z. Charrouf, *Front. Nutr. Sci.*, 2021, **8**, 804587.
24 J. Kim, D. N. Kim, S. H. Lee, S.-H. Yoo and S. Lee, *Food Chem.*, 2010, **118**, 398–402.
25 P. K. Okuro, A. A. Malfatti-Gasperini, A. A. Vicente and R. L. Cunha, *Food Res. Int.*, 2018, **111**, 168–177.
26 Y. Tian and N. C. Acevedo, *Food Chem.*, 2018, **255**, 252–259.
27 S. Guo, M. Song, X. Gao, L. Dong, T. Hou, X. Lin, W. Tan, Y. Cao, M. Rogers and Y. Lan, *Food Funct.*, 2020, **11**, 7651–7660.
28 F. Galli, A. Azzi, M. Birringer, J. M. Cook-Mills, M. Eggersdorfer, J. Frank, G. Cruciani, S. Lorkowski and N. K. Özer, *Free Radical Biol. Med.*, 2017, **102**, 16–36.